Received: 15 February 2023 | Revised: 30 May 2023 | Accepted: 7 June 2023

DOI: 10.1002/suco.202300114

ARTICLE

fib WILEY

The basis for ductility evaluation in SFRC structures in MC2020: An investigation on slabs and shallow beams

Matteo Colombo[1] | **Antonio Conforti**[2] | **Marco di Prisco**[1] | **Bruno Leporace-Guimil**[3] | **Giovanni Plizzari**[2] | **Giulio Zani**[1]

[1]Department of Civil and Environmental Engineering, Politecnico di Milano, Milan, Italy

[2]Department of Civil, Environmental, Architectural Engineering and Mathematics, University of Brescia, Brescia, Italy

[3]Department of Civil and Environmental Engineering, Universitat Politècnica de Catalunya, Barcelona, Spain

Correspondence
Giulio Zani, Department of Civil and Environmental Engineering, Politecnico di Milano, Milan, Italy.
Email: giulio.zani@polimi.it

Funding information
Arcelor-Mittal Europe; Bekaert GmbH

Abstract

The paper presents a synthesis of an extensive experimental campaign on linear and two-dimensional steel fiber reinforced concrete (SFRC) structural elements carried out to check the ductility requirements aimed at guaranteeing limit analysis approaches for the computation of ultimate load-bearing capacity of SFRC structures; special attention is devoted to the role of the degree of redundancy of the structure. In particular, full-scale shallow beams and slabs reinforced with steel fibers (with or without conventional longitudinal reinforcement) were tested in two different laboratories: the Politecnico di Milano (PoliMI) and the University of Brescia (UniBS). In this experimental campaign, two different fiber contents and fiber types were considered. The experimental investigation, carried out within the activities to support Annex L of Eurocode 2, was fundamental also for developing the design rules included in the *fib* Model Code 2020 and allowed to formulate conclusions regarding optimization of the mix design, ductility, and design prediction at the ultimate capacity.

KEYWORDS

bending resistance, elevated slabs, limit analysis, minimum reinforcement, shallow beams, steel fiber reinforced concrete (SFRC)

1 | INTRODUCTION

The new *fib* Model Code for Concrete Structures 2020 (hereafter MC2020) provides guidelines for the design of new concrete structures and the assessment of existing ones. Additionally, it offers insights into their effective life-cycle management (LCM). This ambitious project builds upon the achievements of *fib* MC2010,[1] the previous edition of the *fib* Model Code for Concrete Structures, where fiber reinforced concrete (FRC) was introduced as a new structural material, along with its corresponding design rules. Since then, the use of FRC has gained momentum, particularly in applications such as foundations, tunnel segments, and construction of shallow beams and elevated slabs.

The MC2020 new-rules for FRC structural elements include mixed-mode actions dominated by shear stresses (like shear, punching, and torsion) and mode-I actions (such as uniaxial tension and bending), where crack development and stress redistribution may play a major role, depending on the degree of redundancy of the structural element. The latter is the main aim of the present work, which focuses on the requirements necessary to ensure structural ductility, which is crucial to prevent

brittle failures and to allow the use of limit analysis as a tool to predict the bearing capacity of a structure. The research findings are supported by a comprehensive experimental campaign on the behavior of steel fiber reinforced concrete (SFRC) structural members, with or without conventional reinforcement. The FRC characterization is based on the EN 14651[2] classes introduced in the MC2010.[3] In MC2020, the redistribution factor proposed in MC2010 is improved, switching from a global factor directly applied to the bearing capacity (K_{Rd}) to a new material factor (κ_G) that allows the designer to amplify the FRC contribution only when conventional reinforcement is also present. This approach has been suggested also in the new generation of Eurocodes, which includes a new annex (Annex L) explicitly devoted to the design of SFRC structural elements.[4]

Although some studies are available in the literature on the constitutive relationship of the material,[5–10] on the structural behavior of elevated slabs and beams,[11–16] and on their design approach,[17–19] the present work aims to shed some new lights through a comprehensive experimental campaign on SFRC beams and slabs, with or without ordinary reinforcement. Special attention is devoted to the reliability of building codes requirements to predict both the load-bearing capacity and the behavior in service conditions, with the aim of comparing the ductility supplied by high dosages of steel fibers, or low dosages used in combination with conventional reinforcement.[20]

The experimental campaign aimed to better understand the structural behavior of SFRC structural elements with different degrees of redundancy, both in terms of bearing capacity and ductility. Furthermore, the experimental results will be adopted to validate the approaches proposed by the building codes for structures with limited conventional reinforcement, such as that usually adopted in shallow beams and in elevated slabs.

The experimental campaign was carried out in two research laboratories, namely the Politecnico di Milano (PoliMI, L1) and the University of Brescia (UniBS, L2).

2 | MATERIALS

One reference plain concrete (PC) and four SFRC mixes were adopted for the production of the full-scale specimens; the latter differed for fiber content (i.e., 55 or 70 kg/m^3) and fiber types (denoted as A and B, see Tables 1 and 2). The composition of the five mixes is summarized in Table 1; it can be observed that the base concrete matrix (PC) was the same for all mixes. The properties of the two types of fibers adopted are listed in Table 2, while Table 3 presents the results of the uniaxial tensile tests conducted on six Φ10 and six Φ12 B450C bars (both employed as conventional reinforcement).

TABLE 1 Composition of the different concretes investigated.

Ingredient	PC	55A/55B	70A/70B
Limestone filler (kg/m^3)	160	160	160
Sand 0–3 mm (kg/m^3)	690	690	690
Sand 0–12 mm (kg/m^3)	440	440	440
Gravel 8–15 mm (kg/m^3)	610	610	610
Cement I 52.5R (kg/m^3)	350	350	350
Water/cement ratio (–)	0.49	0.49	0.49
Superplasticiser (L/m^3)	–	7	7.5
Steel fibers (kg/m^3)	–	55	70

TABLE 2 Properties of the steel fibers used.

Fiber property	A	B
Shape	Hooked-end	Hooked-end (double)
Length, l_f (mm)	60	60
Diameter, d_f (mm)	0.9	0.9
Aspect ratio (l_f/d_f)	67	65
Tensile strength (MPa)	1900	2300

TABLE 3 Mechanical characterization of the B450C steel bars.

Steel rebar		f_y (MPa)	f_u (MPa)	ε_{um} (–)
Φ10	Avg	544.4	631.4	0.091
	CV	(1%)	(1%)	(5%)
Φ12	Avg	488.4	578.8	0.100
	CV	(2%)	(1%)	(4%)

The mechanical characterization of the SFRCs was performed through three-point bending tests, according to EN 14651.[2] It is worth noting that the full-scale samples (beams and slabs) with additional traditional reinforcement (55A + R and 55B + R) were cast in a different batch than the samples with fiber reinforcement only (55A and 55B). For this reason, in Table 4, the mechanical properties of specimens 55A, 55B, 55A + R and 55B + R are considered both independently (considering the samples coming from each individual batch) and referred to the nominally identical batches 55A/55A + R and 55B/55B + R.

Experimental results from three-point bending tests (according to EN 14651) are summarized in Figure 1 (mean curves), where the average nominal stress–CMOD curves of each batch are compared. Figure 2 provides a detailed breakdown of the results, differentiating between L1 and L2 laboratories, which represent the two distinct research facilities. The experimental results highlight the importance of a proper production control, since they demonstrate that even when using the same concrete mix with identical fiber content,

TABLE 4 Results of the mechanical characterization tests on notched beams.

Batch	n		$f_{c,cube}$ (MPa)	$f_{ct,fl}$ (MPa)	f_{R1} (MPa)	f_{R2} (MPa)	f_{R3} (MPa)	f_{R4} (MPa)	Class (EC2)
55A	12	Avg	75.81	6.29	9.36	10.85	10.73	10.36	5d
		CV	2.7%	11.0%	23.0%	18.0%	12.0%	10.0%	
55A + R	12	Avg	79.47	6.15	8.58	10.19	10.21	9.91	5d
		CV	4.4%	13.0%	13.0%	12.0%	10.0%	11.0%	
55B	12	Avg	74.62	5.66	7.23	8.93	8.98	7.42	4e
		CV	3.8%	13.0%	24.0%	21.0%	20.0%	23.0%	
55B + R	12	Avg	76.35	5.48	5.35	7.08	6.99	6.04	2.5e
		CV	2.3%	7.0%	33.0%	33.0%	27.0%	29.0%	
55A/ 55A + R	24	Avg	77.64	6.22	8.97	10.52	10.47	10.13	5d
		CV	4.3%	11.7%	19.3%	15.3%	11.0%	10.7%	
55B/ 55B + R	24	Avg	75.48	5.57	6.33	8.05	8.03	6.76	3e
		CV	3.2%	13.0%	27.4%	20.0%	14.4%	16.0%	
70A	12	Avg	71.70	6.50	9.53	10.49	10.54	9.88	5d
		CV	2.9%	6.0%	19.0%	14.0%	14.0%	15.0%	
70B	12	Avg	73.74	6.31	9.54	11.90	11.77	9.73	5e
		CV	3.3%	9.0%	18.0%	12.0%	8.0%	12.0%	
PC	12	Avg	67.79	5.46	0.41	–	–	–	–
		CV	3.3%	12.0%	22.0%	–	–	–	

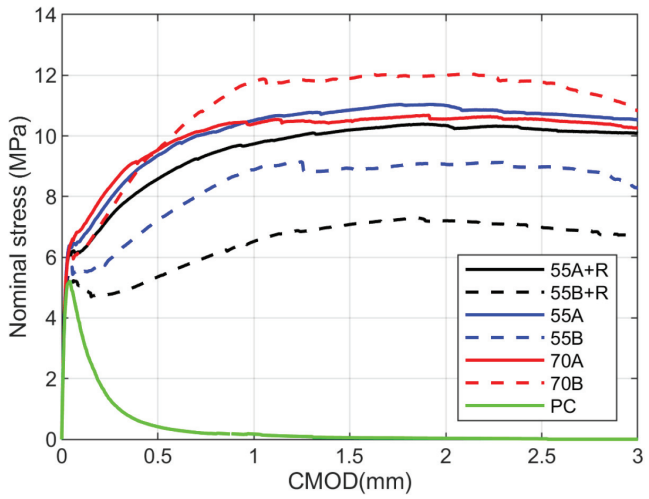

FIGURE 1 Results of the EN 14651 characterization tests (average values).

different performance can be observed if samples are obtained from separate batches.

After testing EN 14651 specimens, the distribution of fibers was also evaluated in the cracked surface by considering three equal areas (i.e., A, B and C in Figure 3). As reported in Table 5, the fiber density (fibers per unit area) for each batch shows a good fiber distribution. As expected, the fiber density significantly influences the post-cracking residual strength (i.e., the greater the fiber density, the higher the nominal post-cracking residual strength; see Figure 4).

3 | FULL-SCALE TESTS ON SHALLOW BEAMS

The full-scale tests were performed on beams 0.12 m thick, 3 m long, and 0.6 m wide. Materials 55A and 55B were tested only in combination with traditional longitudinal reinforcement, while materials 70A and 70B were tested in specimens without longitudinal rebars. Furthermore, it should be noted that a reference traditional solution in reinforced concrete (RC) was also considered. The distance between the centre of conventional reinforcement and the bottom of the beam was equal to 30 mm. The overview of the full-scale beams test campaign, including specification of the reinforcement in the different samples, is summarized in Table 6 and Figure 5. The beams were tested in a four-point bending scheme and the tests were performed under displacement control.

The loading scheme, as well as the instrumentation adopted, are represented in Figures 5 and 6. As already discussed for the material characterization tests, some of the tests were performed by the PoliMI lab (L1) and some by the UniBS lab (L2).

The results of the beam tests are exhibited in Figure 7 in terms of applied load (P) versus mid-span displacement, assumed as the average value between displacements δ_1 and δ_2 (Figure 5). Final crack patterns are shown in Figure 8. The main experimental results from shallow beams are summarized in Table 7, where P_{cr} represents the cracking

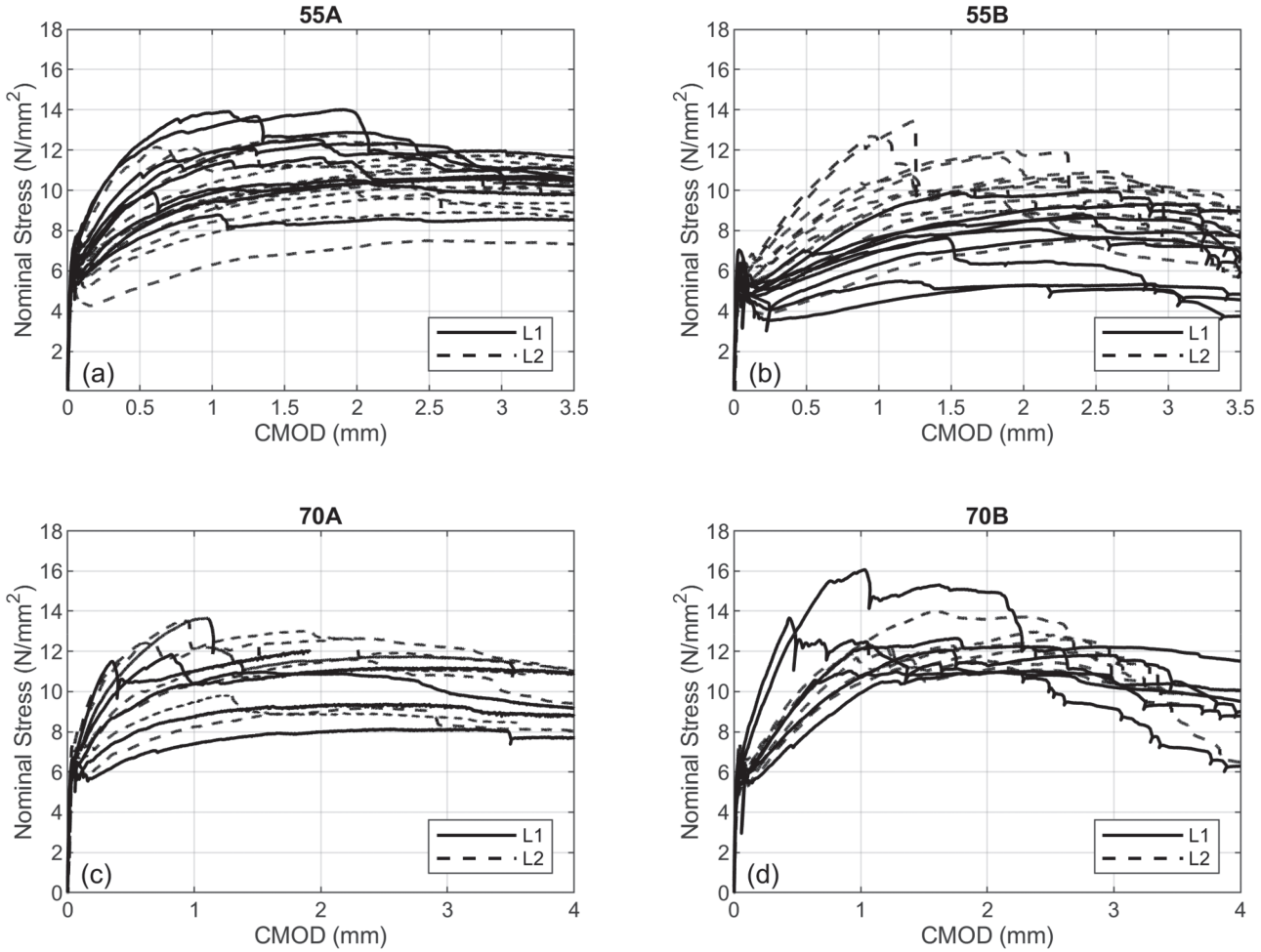

FIGURE 2 Results of the EN 14651 characterization tests (labs L1 and L2): (a) material 55A, (b) material 55B, (c) material 70A, and (d) material 70B.

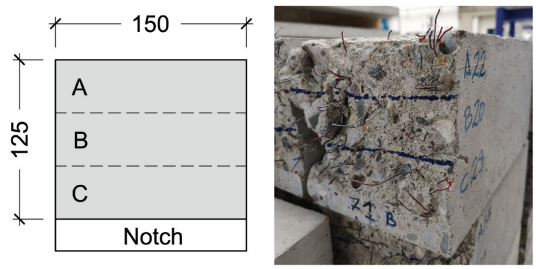

FIGURE 3 EN 14651 beams: definition of areas (A, B, and C) on the cracked surface (nominal measures expressed in mm).

load, δ_{cr} the cracking mid-span displacement, and P_{max} and δ_{max} are respectively the load and the mid-span displacement at the peak of the experimental response.

It is worth noticing that nominally identical beams showed similar trends, with the exception of specimen 55B + R-2, which had a sudden collapse during the post-peak branch (the final unloading branch is missing because the beam uncontrollably broke into two pieces).

All the beams exhibited similar responses in the pre-cracking branch, as confirmed by the rather constant values of cracking load P_{cr} (with the only exception of beam 55B + R-3, which exhibited first cracking at a lower load). Hybrid solutions with both fibers and ordinary reinforcement experienced higher ductility than solutions reinforced with fibers only; in fact, sets 70A and 70B exhibited the lowest P_{max}/P_{cr} and δ_{max}/δ_{cr} ratios.

It can be generally stated that the hybrid solutions (55B + R) exhibited the best performance in bending behavior of fiber-reinforced shallow beams.

Figure 7 also highlights, for each test type, the load corresponding to the ultimate resistant moment computed with a rigid plastic model in tension for FRC, using a stress-block constitutive law in compression and assuming that longitudinal reinforcement, when available, was yielded (Figure 9). The ultimate loads P_R of Table 8 were computed considering both design (Des) and average (Avg) values of the material properties. For the design load level, the κ_0 and κ_G coefficients, accounting for orientation and for structural redistribution, respectively, were both conservatively set equal to 1.

TABLE 5 Distribution of fibers at different locations on the cracked surface (CV in brackets).

Batch	Lab	A (no. fibers/cm^2)	B (no. fibers/cm^2)	C (no. fibers/cm^2)	Mean (no. fibers/cm^2)
55A	L1	0.84 (17%)	0.86 (14%)	0.91 (12%)	0.87 (8%)
	L2	0.66 (31%)	0.75 (19%)	0.60 (31%)	0.67 (24%)
55B	L1	0.44 (25%)	0.49 (25%)	0.45 (24%)	0.46 (18%)
	L2	0.82 (19%)	0.76 (25%)	0.70 (9%)	0.76 (12%)
70A	L1	0.75 (38%)	0.73 (31%)	0.89 (15%)	0.79 (22%)
	L2	0.80 (24%)	0.84 (35%)	0.81 (17%)	0.82 (21%)
70B	L1	1.07 (6%)	0.94 (13%)	1.02 (24%)	1.01 (9%)
	L2	0.74 (16%)	0.83 (13%)	0.74 (12%)	0.77 (5%)
55A + R	L1	0.76 (22%)	0.79 (17%)	0.83 (23%)	0.79 (14%)
	L2	0.56 (23%)	0.66 (10%)	0.68 (18%)	0.63 (9%)
55B + R	L1	0.42 (23%)	0.38 (51%)	0.43 (66%)	0.41 (42%)
	L2	0.51 (32%)	0.52 (36%)	0.51 (32%)	0.51 (33%)

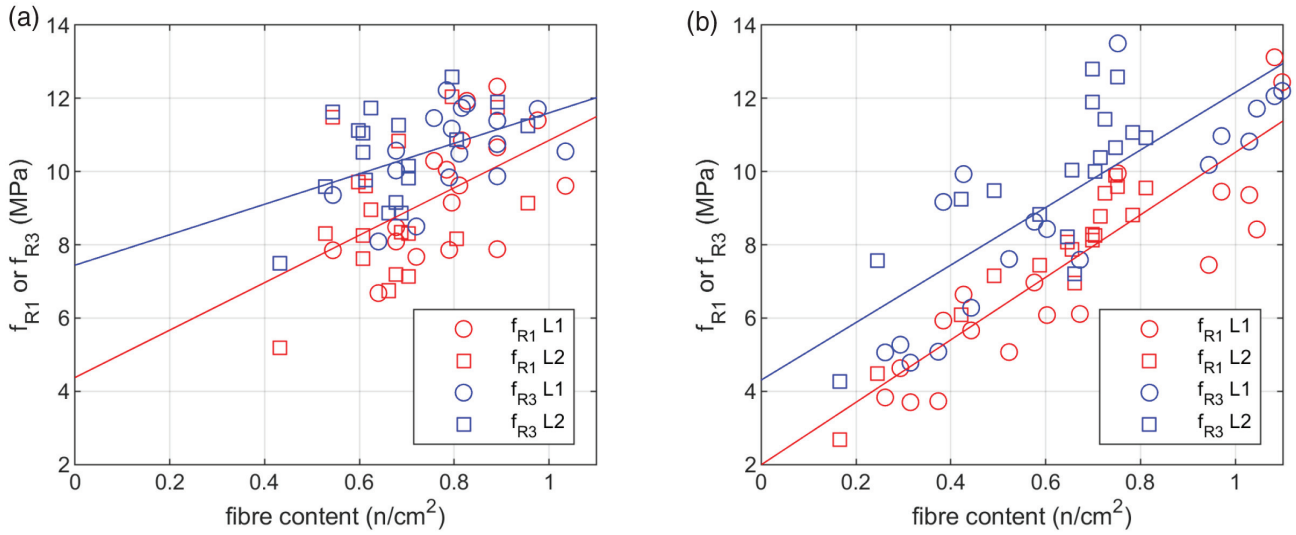

FIGURE 4 Equivalent strength versus the number of fibers in the cracked section.

TABLE 6 Reinforcement of the shallow beams.

Beam	Number of tests	Longitudinal reinforcement	ρ_s	Amount of longitudinal reinforcement steel (kg/m^3)	Amount of fiber steel (kg/m^3)
RC	3	2Φ12 + 1Φ10	0.56%	33	–
55A + R	3	2Φ10	0.29%	17	55
55B + R	3	2Φ10	0.29%	17	55
70A	3	–	–	–	70
70B	3	–	–	–	70

It is worth noting that the design strength consistently remains on the safe side. In all cases, the choice of material safety factors (1.15 for steel and 1.5 for FRC) results in an ultimate design load that is below the recorded experimental values. This observation holds true for the most critical test sample (55A + R-1) as well, which demonstrates a peak load 5% higher than the analytically estimated ultimate design load. Therefore, it can be concluded that the design procedure, based on the tests discussed in this work, provides a conservative estimate.

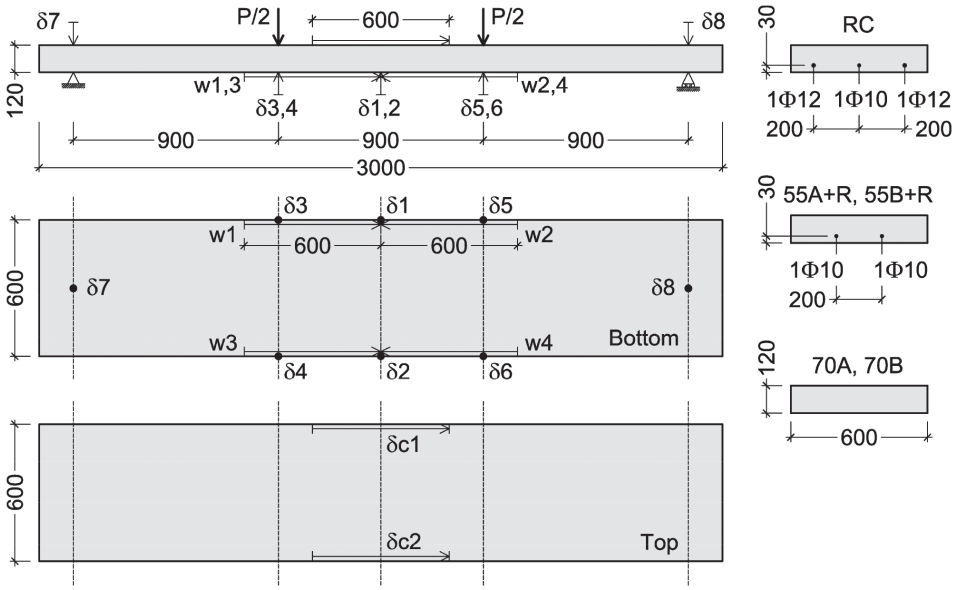

FIGURE 5 Experimental set-up and instrumentation adopted for the bending tests on shallow beams (nominal measures expressed in mm).

FIGURE 6 Bending tests on shallow beams: (a) lab L1 and (b) lab L2.

It should be observed that the load-bearing capacity of SFRC beams (without rebars) is comparable with that of the reference solution (RC). On the contrary, the ductility of the structural solutions with fiber reinforcement only is limited; in fact, although the combination with a small amount of longitudinal reinforcement (158 mm^2 against a minimum reinforcement—without fibers—of about 400 mm^2 considering a design yield stress $f_{yd} = 391$ MPa) can provide a certain ductility, the latter is always lower than that exhibited by the traditional RC solution. This observation becomes even more evident when considering the reinforcement ratios ρ_F: if we consider the cases with 55 kg/m^3 of fibers and an orientation factor $\kappa_0 = 1$ (random 3D distribution), we obtain an equivalent ρ_F equal to 0.32%. When combined with the 0.29% provided by the two Φ10, the total ρ_F becomes comparable to the 0.56% of the RC solution; in contrast, 70 kg/m^3 of fibers correspond to 0.44%, which is lower than the 0.56% of the RC solution.

The tests also allowed to assess the average crack spacing, which represents an important parameter for structural design both at serviceability limit states (since it governs durability), and at ultimate limit states (as it governs the characteristic length of FRC in tension and influences its stress–strain uniaxial tensile law). The experimental crack spacings $s_{rm,exp}$ are listed in Table 7, together with those computed according to the last drafts of MC2020[21] and Annex L of Eurocode 2[22] referring to class values of the material properties. In the calculation of crack spacing, beams without longitudinal reinforcement are excluded. This is because the applicable codes provide guidelines for selecting a characteristic length, but they do not specify whether it should always be directly linked to crack spacing.

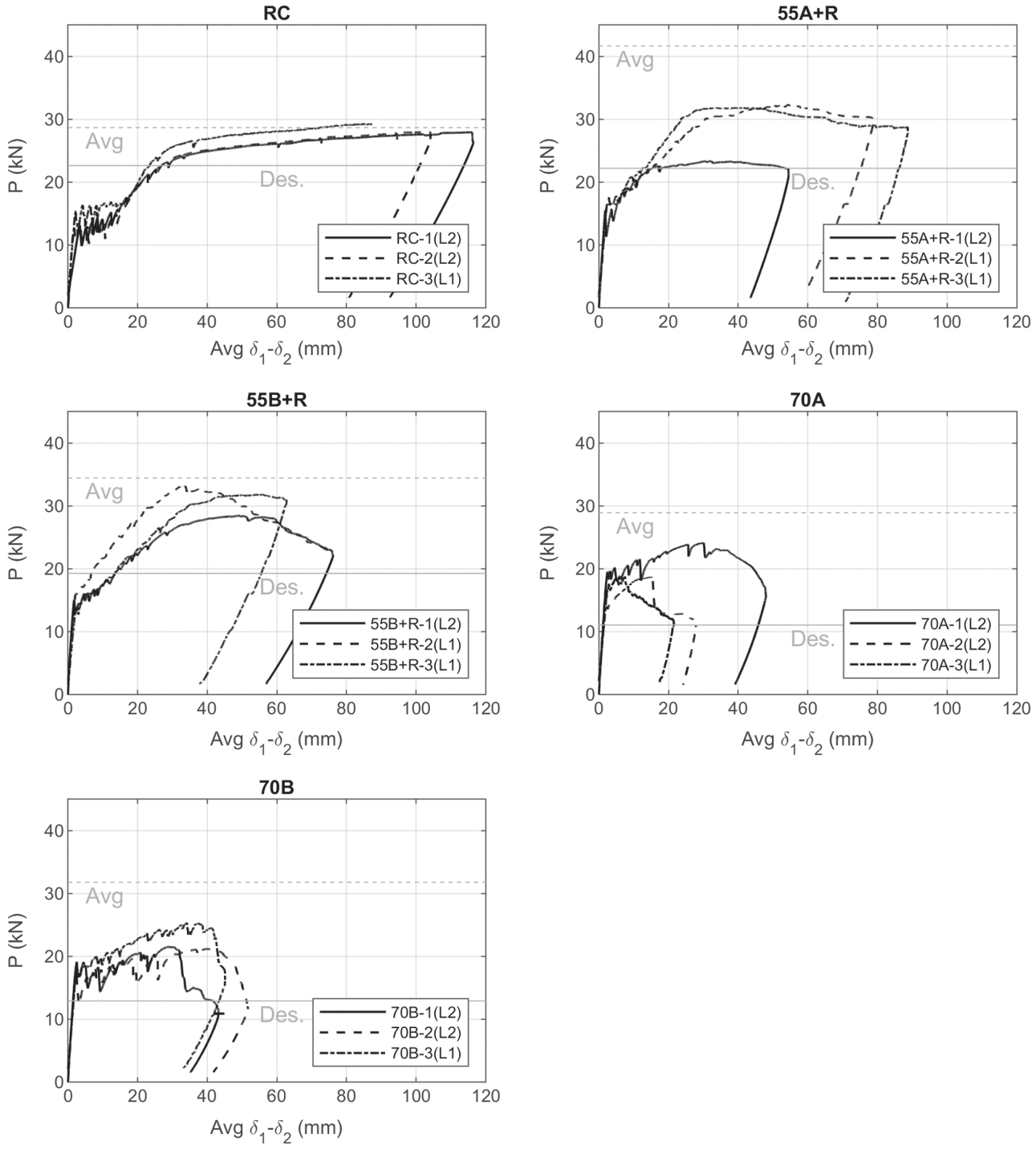

FIGURE 7 Diagrams of the load versus mid-span displacement from bending tests on shallow beams. Please note that in the RC (reinforced concrete) specimens, the tests were terminated before failure, and in all other cases, after reaching the peak and determining a softening behavior, unloading was performed to prevent sudden collapses.

In the MC2020 the average crack spacing s_{rm} is calculated as:

$$s_{rm} = \left(1.5 \cdot c + k_{\phi/\rho} \cdot k_{fl} \cdot k_b \frac{(f_{ctm} - f_{Fts,ef}) \cdot \phi}{\tau_{bms} \cdot \rho_{s,ef}}\right). \quad (1)$$

Equation (1) is based on the principle of force equilibrium between the tensile strength of the concrete and the strength of the reinforcement. When the crack spacing increases significantly, the structural characteristic length l_{cs}, typically represented by s_{rm}, is limited by the distance $y = (h - x)$ between the neutral axis and the tensile side of

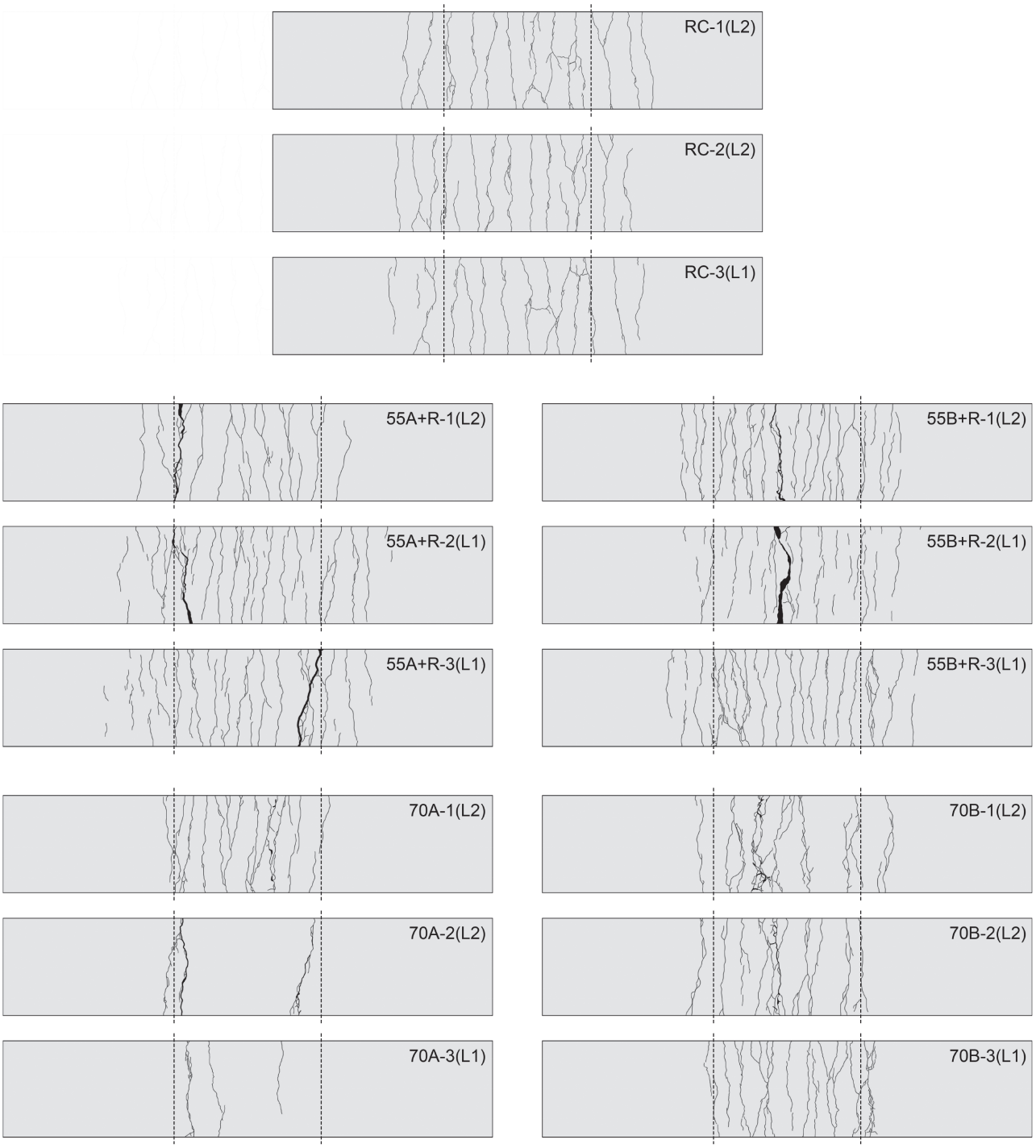

FIGURE 8 Final crack pattern on the bottom surfaces of the shallow beams. The position of the loading knives is represented by the two dashed lines.

the cross-section. The limitation occurs because the phenomenon is no longer governed by equilibrium, but rather associated with the curvature of the section. Note that in computing s_{rm} the identification of the position x of the neutral axis was simplified by assuming the one shown in Figure 9. For the beams investigated, $k_b = 0.9$, $k_{fl} = 40/120 = 0.33$ and $k_{\phi/\rho}/\tau_{bms} = 1/7.2$ were considered.

In the Annex L of Eurocode 2 the mean crack spacing $s_{r,m,cal,F}$ is defined as:

$$s_{r,m,cal,F} = \begin{cases} 1.5 \cdot c + \dfrac{k_{fl} \cdot k_b}{7.2} \cdot \dfrac{\phi}{\rho_{p,ef}} \cdot (1 - \alpha_f) & \text{for } s \le 10\phi \\ (h - x) & \text{for } s > 10\phi \end{cases}, \quad (2)$$

TABLE 7 Main experimental results from bending tests on shallow beams.

Beam	Lab	P_{cr} (kN)	δ_{cr} (mm)	P_{max} (kN)	δ_{max} (mm)	P_{max}/P_{cr} (−)	δ_{max}/δ_{cr} (−)	$s_{rm,exp}$ (mm)	$s_{r,m,cal,F}$[d] (mm)	s_{rm}[e] (mm)
RC-1[a]	L2	12.7	1.63	28.0[a]	103.8[a]	2.2[a]	63.7[a]	110	109.1[b]	94.8
RC-2[a]	L2	13.1	3.16	27.9[a]	112.2[a]	2.1[a]	35.5[a]	102		
RC-3[a]	L1	15.5	2.21	29.2[a]	87.2[a]	1.9[a]	39.5[a]	114		
55A + R-1	L2	15.5	1.65	23.3	31.5	1.5	19.1	99	107.2	64.9
55A + R-2	L1	17.6	2.84	32.4	53.0	1.8	18.7	83		
55A + R-3	L1	16.5	2.80	31.8	42.9	1.9	15.3	80		
55B + R-1	L2	15.0	1.63	28.4	50.4	1.9	30.9	83	109.2	73.9
55B + R-2	L1	16.0	2.24	33.2	33.0	2.1	14.7	77		
55B + R-3	L1	13.9	2.32	31.8	55.9	2.3	24.1	75		
70A-1	L2	19.5	2.33	24.1	29.9	1.2	12.8	81	(112.5)	(112.5)
70A-2	L2	17.6	1.99	18.7	13.0	1.1	6.5	–		
70A-3	L1	17.5	2.84	18.7	7.5	1.1	2.6	400[c]		
70B-1	L2	19.1	2.36	21.5	28.1	1.1	11.9	94	(111.2)	(111.2)
70B-2	L2	17.4	2.19	21.2	40.1	1.2	18.3	81		
70B-3	L1	18.0	2.72	25.4	34.1	1.4	12.5	80		

Note: Estimated crack spacings of specimens 70A and 70B are displayed in brackets, since the values correspond formally to a characteristic length and may be considered as an estimate of crack spacing only when multiple cracks are developed (70A-1, 70B-1, 70B-2, 70B-3 in Figure 8).

[a]Test terminated before failure (the maximum load and maximum displacement could be higher).

[b]The reported value is an $s_{r,m,cal}$.

[c]In this test only three cracks propagated.

[d]EC2-Annex L.

[e]MC2020.

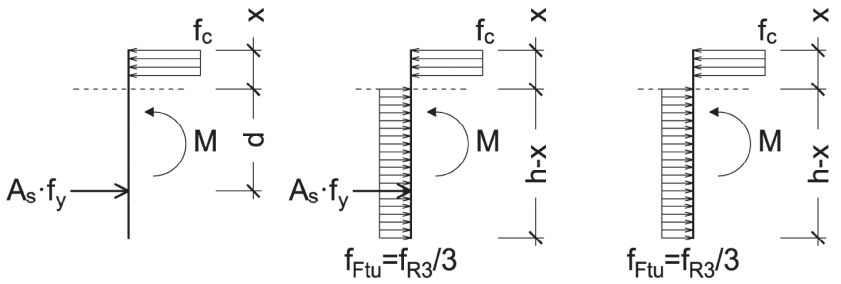

FIGURE 9 Simplified sectional equilibriums adopted for estimating ultimate loads based on average and design strengths of materials; from left to right: reinforced concrete (RC) section, hybrid section (fibers and rebar), and fiber-reinforced concrete (FRC) section.

where s is the spacing of the bonded reinforcement in the tension zone. Considering that:

$$\alpha_f = \frac{(0.37 \cdot \kappa_0 \cdot \kappa_G \cdot f_{R1k})}{f_{ctm}} \leq 1.0, \quad (3)$$

the similarity between the two approaches can be observed.

In the Annex L of Eurocode 2, the average crack spacing is always determined by the value $(h-x)$, as the longitudinal bars are spaced at least 10 times the diameter (10Φ) apart. On the contrary, in MC2020, the upper limit only applies in the evaluation of the characteristic length of SFRC solutions without any rebar. The comparison of Table 7 shows how the new formulation suggested in the Annex L provides a more cautious estimation of the average crack distance as compared to that suggested by the last draft of the MC2020.

TABLE 8 Prediction of the ultimate load of the beams based on sectional analysis.

Beam	Lab	P_{max} (kN)	Predicted ultimate load P_R		P_{max}/P_{Rd} (−)
			P_{Rd} Des. (kN)	P_{Rm} Avg. (kN)	
RC-1[a]	L2	28.0[a]	22.6	28.7	1.24[a]
RC-2[a]	L2	27.9[a]			1.23[a]
RC-3[a]	L1	29.2[a]			1.29[a]
55A + R-1	L2	23.3	22.2	41.7	1.05
55A + R-2	L1	32.4			1.46
55A + R-3	L1	31.8			1.43
55B + R-1	L2	28.4	19.3	34.4	1.47
55B + R-2	L1	33.2			1.72
55B + R-3	L1	31.8			1.65
70A-1	L2	24.1	11.0	28.9	2.19
70A-2	L2	18.7			1.70
70A-3	L1	18.7			1.70
70B-1	L2	21.5	12.9	31.8	1.67
70B-2	L2	21.2			1.64
70B-3	L1	25.4			1.97

[a]Test terminated before failure (the maximum load could be higher).

TABLE 9 Reinforcement of the slab specimens.

Slab	Number of tests	Longitudinal reinforcement	Amount of longitudinal reinforcement steel (kg/m^3)	Amount of fiber steel (kg/m^3)
55A + R	2	2Φ12 + 1Φ10	33	55
55B + R	2	2Φ12 + 1Φ10	33	55
55A	2	–	–	55
55B	2	–	–	55
70A	2	–	–	70
70B	2	–	–	70

4 | FULL-SCALE TESTS ON ELEVATED SLABS

The tests performed on slabs are summarized in Table 9. The detailing of the traditional reinforcement adopted in 55A + R and 55B + R tests is represented in Figure 10. For each type of slab, two nominally identical tests were performed (Figure 11): one at PoliMI (L1) and one at UniBS (L2).

The slabs in the study were simply supported at four corners and loaded by a central load; the support and load areas had a square shape with dimensions of 200 mm × 200 mm in the plane of the slab. The tests were displacement-controlled, considering load point displacement as a feedback parameter. The details of the instrumentation adopted during the tests are shown in Figures 10 and 11.

Experimental results are exhibited in Figure 12 in terms of load versus central displacement (under the load point). Further experimental information from slab tests are reported in Table 10, while the final crack patterns are displayed in Figures 13 and 14. In Figure 12, for each type of slab, the ultimate load $P_R^{(a)}$ computed according to the yield line approach is also represented, assuming the kinematic mechanisms shown in Figure 15a. In this computation, the resistant bending moment of the cross-section has been evaluated, as already discussed for the beams, considering a rigid plastic constitutive law for FRC in tension, a stress-block in compression, and an elastoplastic constitutive law for traditional reinforcement steel

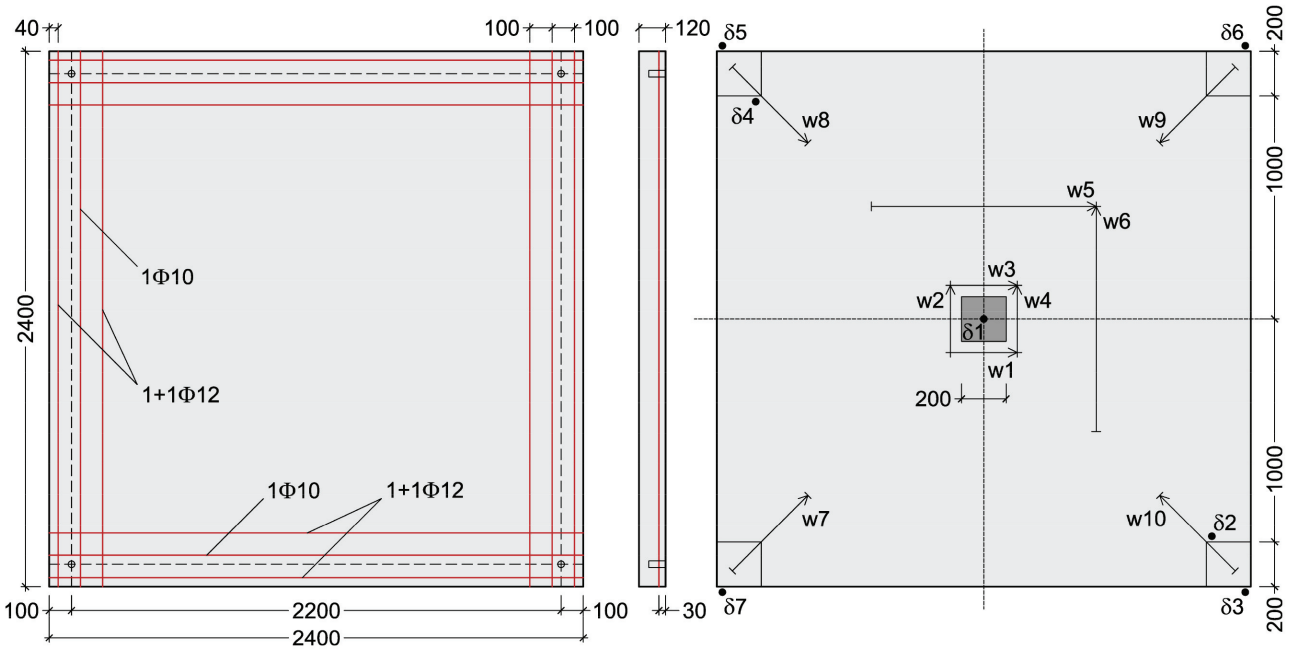

FIGURE 10 Detail of the conventional reinforcement adopted in the slab tests denoted as 55A + R and 55B + R (left) and instrumentation adopted for the slab tests (right). Nominal measures are expressed in mm.

FIGURE 11 Full-scale tests on slabs: (a) lab L1 and (b) lab L2.

(Figure 9). The two horizontal lines in each diagram in Figure 12 represent the yield line load $P_R^{(a)}$ computed considering design (Des.) and average (Avg.) values for the materials resistances. It is worth noting that in the computation of the resistant bending moment, when considering material design values, the κ_G factor is applied to the design strength, as proposed by the last drafts of *fib* MC2020 and Eurocode 2-Annex L. For a squared slab, the following equation applies, where A_{ct} is the cracked area of the structure (expressed in m^2), neglecting the specific redistribution capacity of the structure:

$$\kappa_G = 1 + 0.5 \cdot A_{ct} \leq 1.5. \quad (4)$$

When considering the average material properties to calculate the resistant bending moment, the unit value of κ_G factor is adopted.

It can be observed that the global safety coefficient obtained with the yield line theory is always larger than 1.5 (Figure 15a), which corresponds to the material partial safety factor (γ_F) prescribed by design codes. Hence, it may be concluded that the design procedure proposed

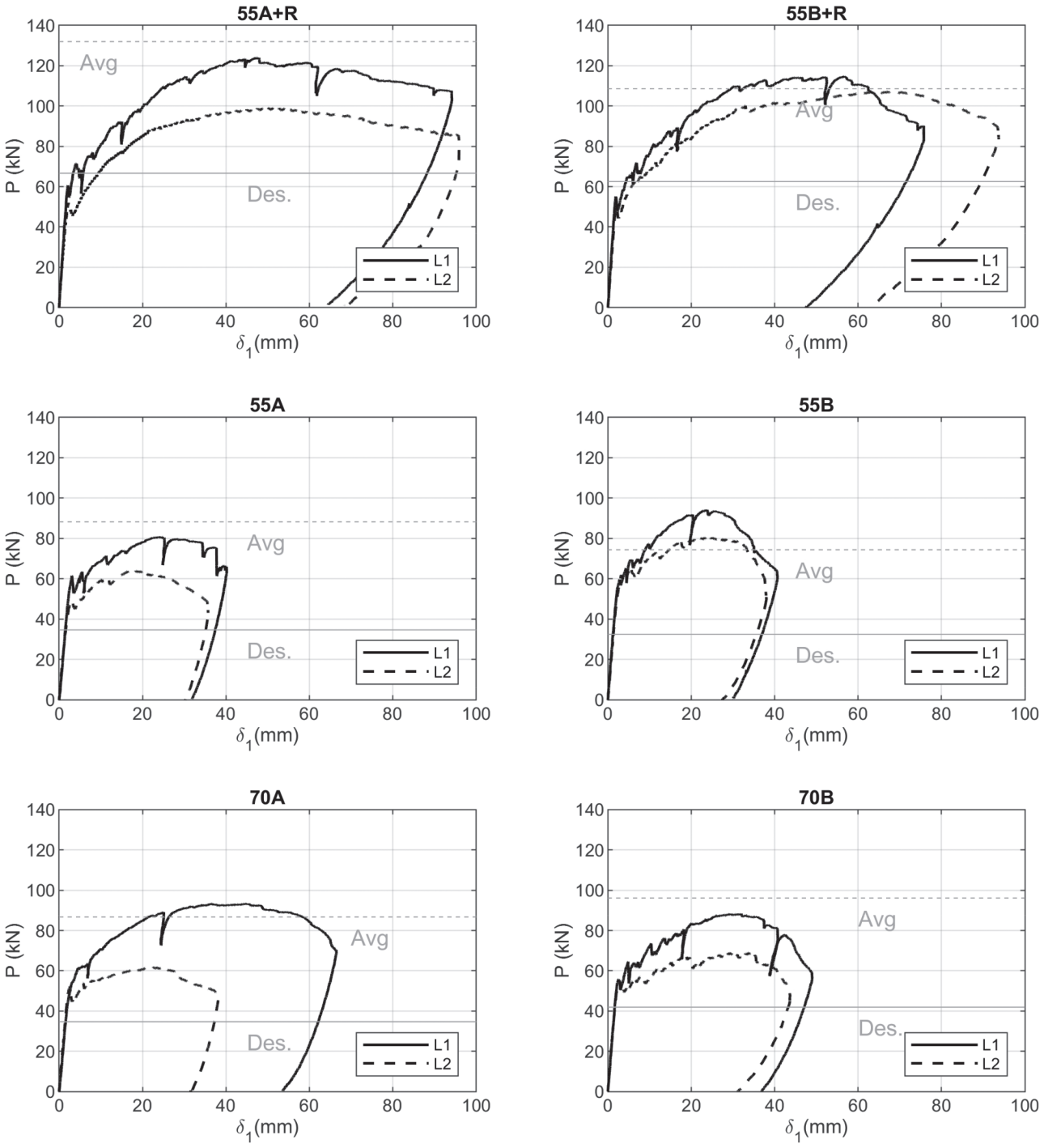

FIGURE 12 Experimental diagrams of the load versus the mid-point displacement of the slabs.

leads to elevated slabs that comply with safety requirements.

It can be noticed that the experimental results show different responses for the tests conducted at the two different labs. The main difference can be explained by the top-slab cracks at the corner supports in L1 tests; this disparity could be due to variations in the stiffness of the supporting legs in the two different experimental setups. The influence of top-slab cracks can be estimated with the yield line scheme presented in Figure 15b (top-slab cracks are displayed in red). By adopting this second scheme, a load increment of similar magnitude to the experimental results (with respect to the situation of Figure 15a, see Table 11) can be observed.

TABLE 10 Main experimental results from the slab tests.

Slab	Lab	P_{cr} (kN)	P_{max} (kN)	$\frac{P_{max}}{P_{cr}}$	δ_{cr} (mm)	δ_{max} (mm)	$\delta_{0.85Pmax}$ (mm)	$\frac{\delta_{max}}{\delta_{cr}}$	$\frac{\delta_{0.85Pmax}}{\delta_{cr}}$
55A	L1	61.5	80.9	1.31	3.04	24.5	37.8	8.0	12.4
	L2	47.6	62.9	1.32	2.69	16.9	31.3	6.3	11.6
55B	L1	59.6	94.2	1.58	2.83	23.7	34.0	8.4	12.0
	L2	60.2	79.4	1.32	3.29	23.7	35.4	7.2	10.8
70A	L1	54.1	93.4	1.73	3.10	36.9	63.2	11.9	20.4
	L2	49.4	60.5	1.22	2.64	22.0	33.9	8.3	12.9
70B	L1	55.4	88.4	1.59	2.60	32.0	44.0	12.3	16.9
	L2	53.0	68.1	1.28	2.85	30.4	40.7	10.7	14.3
55A + R	L1	60.6	123.8	2.04	2.11	48.0	94.2	22.7	44.5
	L2	50.7	98.0	1.93	2.33	51.8	95.8	22.2	41.1
55B + R	L1	55.1	114.6	1.86	2.11	56.6	68.4	26.8	32.3
	L2	48.6	105.9	2.18	2.05	67.6	92.3	33.0	45.0

Note: $\delta_{0.85Pmax}$ represents a conventional displacement at failure, determined by considering a 15% reduction in the peak load.

5 | CONCLUDING REMARKS

The results of bending tests carried out on full-scale shallow beams and elevated slabs and the related design predictions according to the rules of the coming *fib* Model Code (MC2020) and Annex L of Eurocode 2, allow drawing the following conclusions:

- The increase of the fiber content does not lead to an increase of the performance class mainly due to fiber distribution, which remains the key parameter to be controlled.
- The use of steel fibers in combination with traditional reinforcement (i.e., hybrid solution) in shallow beams allows to reach similar bearing capacity of RC beams, but the ductility is generally reduced. This finding is explained by the increased heterogeneity introduced in the mechanical response by fibers addition (being randomly distributed within the volume they can potentially lead to localization effects occurring at yielding of longitudinal reinforcement) and suggests to use a minimum longitudinal reinforcement also in the hybrid beams, to prevent any loss of ductility in relation to the RC solution.
- In shallow beams including conventional reinforcement it is observed that the application of the Annex L of Eurocode 2 consistently results in an average crack spacing determined by the value $(h-x)$, which provides in any case a good estimation. On the contrary, in the MC2020, a different approach is adopted where the upper limit of $(h-x)$ applies only in the calculation of the characteristic length for SFRC solutions that do not contain any traditional reinforcement.
- The design prediction of the ultimate capacity of shallow beams and slabs shows that, in both cases, the design procedure provides a conservative estimate of the maximum experimental loads. In slabs, the limit analysis based on the yield line theory allows for a global safety coefficient that exceeds the partial safety factors adopted for the materials. It is evident the beneficial effect exerted by perimetric reinforcement on the ductility of the slab, which is required by both the coming MC2020 and Annex L of EC2 where, to ensure robustness, a minimum reinforcement connecting all the columns is always required.
- The minimum reinforcement in SFRC plates can be reduced to 50% of that prescribed for conventional RC slabs.

It is worth noting that in this experimental investigation on beams the shear contribution of the steel fibers

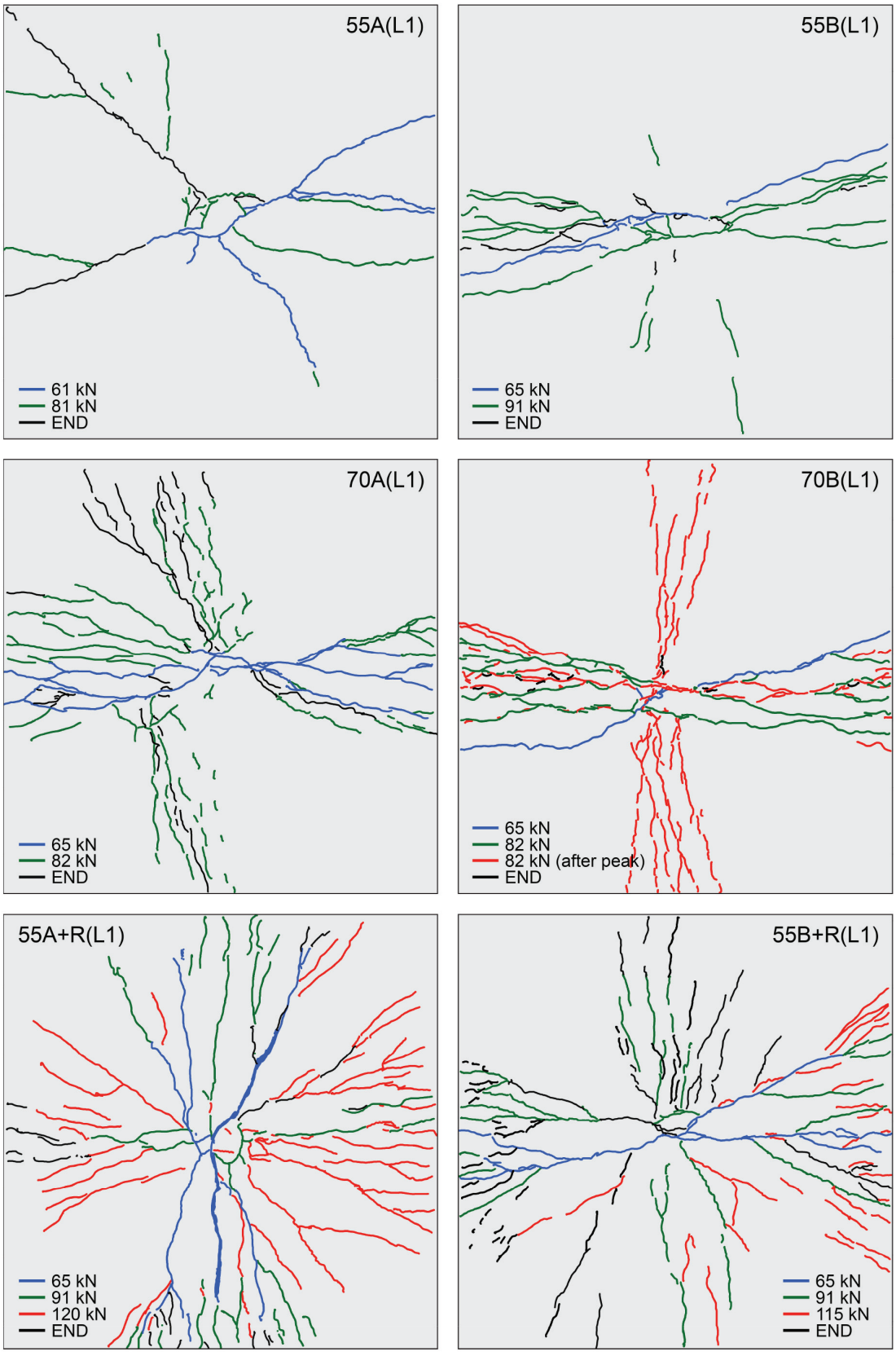

FIGURE 13 Crack pattern on the bottom surfaces of the elevated slabs (lab L1). Note that different colors are associated with different load levels reached during the tests.

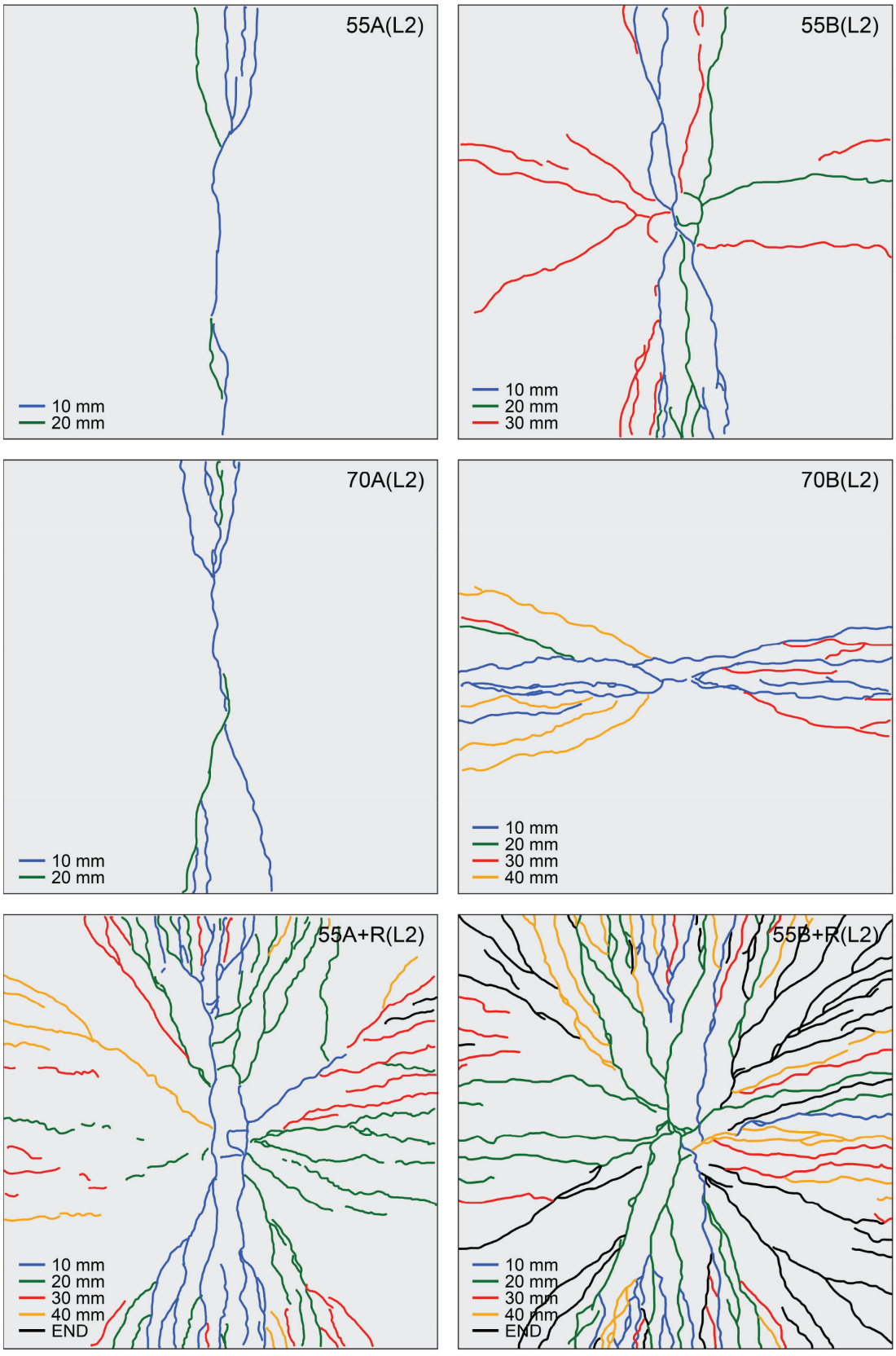

FIGURE 14 Crack pattern on the bottom surfaces of the elevated slabs (lab L2). Note that different colors are associated with different mid-point vertical displacements reached during the tests.

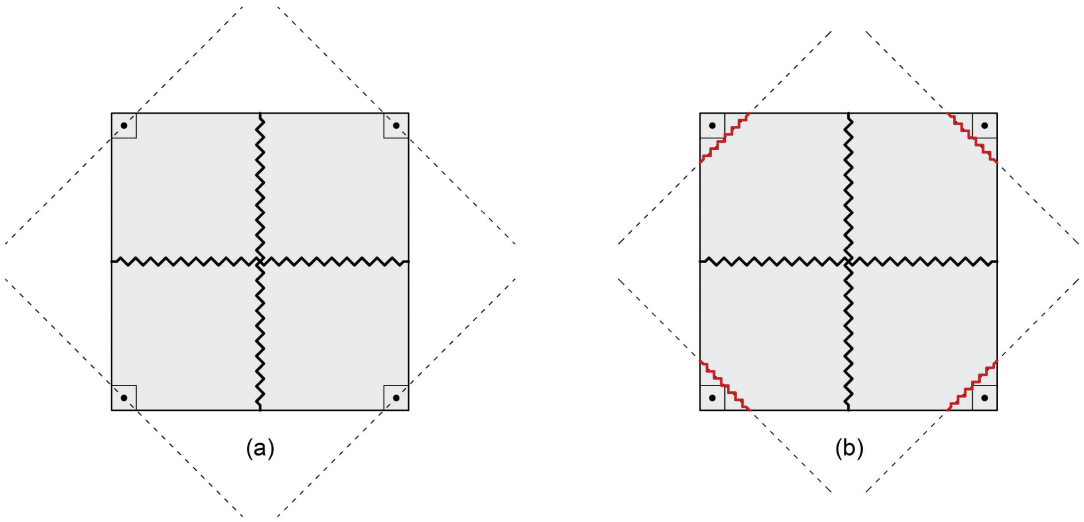

FIGURE 15 Yield line path adopted for resistance computation of elevated slabs: (a) reference scheme providing the values reported in Figure 12; and (b) alternative scheme that incorporates the presence of top-slab cracks at the corners (depicted in red).

TABLE 11 Prediction of the ultimate load of the slabs based on the yield line theory.

			$P_R^{(a)}$ (Figure 15a)		$P_R^{(b)}$ (Figure 15b)		
Slab	**Lab**	P_{max} (kN)	$P_{Rd}^{(a)}$ Des. (kN)	$P_{Rm}^{(a)}$ Avg. (kN)	$P_{Rd}^{(b)}$ Des. (kN)	$P_{Rm}^{(b)}$ Avg. (kN)	$P_{max}/P_{Rd}^{(a)}$ (−)
55A	L1	80.9	34.7	88.2	54.7	98.0	2.33
	L2	62.9					1.81
55B	L1	94.2	32.5	74.4	51.5	84.7	2.90
	L2	79.4					2.44
70A	L1	93.4	34.7	86.7	54.7	96.4	2.69
	L2	60.5					1.74
70B	L1	88.4	41.9	96.1	65.3	106.7	2.11
	L2	68.1					1.63
55A + R	L1	123.8	66.6	118.9	87.2	131.8	1.86
	L2	98.0					1.47
55B + R	L1	114.6	62.5	94.7	81.0	105.1	1.83
	L2	105.9					1.69

was not considered, but it could play a significant role in the definition of the competitiveness of FRC for these kinds of structural elements.

ACKNOWLEDGMENTS

The experimental campaign was financially supported by the Companies Bekaert GmbH and Arcelor-Mittal Europe in the framework of the Committee WG1/SC2/TC250. The authors would like to thank in particular Sebastien Wolf and Elena Vidal Sarmiento for their precious contribution to the discussion of the results.

CONFLICT OF INTEREST STATEMENT

The authors declare no conflicts of interest.

DATA AVAILABILITY STATEMENT

The data that support the findings of this study are available from the corresponding author upon reasonable request.

ORCID

Matteo Colombo https://orcid.org/0000-0001-6457-7894
Antonio Conforti https://orcid.org/0000-0003-2796-7409
Marco di Prisco https://orcid.org/0000-0003-1779-2449
Bruno Leporace-Guimil https://orcid.org/0000-0003-1143-0076
Giovanni Plizzari https://orcid.org/0000-0003-2897-4969
Giulio Zani https://orcid.org/0000-0001-9794-7820

REFERENCES

1. fib. fib Model Code for Concrete Structures 2010, Lausanne, editor. Model code for concrete structures 2010. Berlin: Ernst & Sohn; 2013.
2. EN 14651 Test method for metallic fiberedconcrete – measuring the flexural tensile strength (limit of proportionality (LOP), residual). Brussels: 2004.
3. di Prisco M, Colombo M, Dozio D. Fibre-reinforced concrete in fib model code 2010: principles, models and test validation. Struct Concr. 2013;14(4):342–61.
4. di Prisco M, Kanstad T, Plizzari G, Minelli F, Haus A. Eurocode 2 – annex L – European harmonized standard for steel fibre reinforced concrete. In Serna P, Llano-Torre A, Martí-Vargas JR, Navarro-Gregori J. (eds), Fibre reinforced concrete: improvements and innovations II. BEFIB 2021. RILEM bookseries, Springer, Cham. 36:2022. https://doi.org/10.1007/978-3-030-83719-8_47
5. De La Rosa Á, Ruiz G, Poveda E. Study of the compression behavior of steel-fiber reinforced concrete by means of the response surface methodology. Appl Sci. 2019;9(24):5330.
6. Ruiz G, De La Rosa Á, Poveda E. Relationship between residual flexural strength and compression strength in steel fiber reinforced concrete within the new Eurocode 2 regulatory framework. Theor Appl Fract Mech. 2019;103:102310.
7. Ruiz G, De La Rosa Á, Wolf S, Poveda E. Model for the compressive stress–strain relationship of steel fiber-reinforced concrete for non-linear structural analysis. Hormig Acero. 2018;69(1):75–80.
8. Martinelli P, Colombo M, Pujadas P, de la Fuente A, Cavalaro S, di Prisco M. Characterization tests for SFRC elevated slabs: identification of fibre distribution and orientation effects. Mater Struct. 2021;54:3.
9. Laranjeira F, Grünewald S, Walraven J, Blom C, Molins C, Aguado A. Characterization of the orientation profile of steel fiber reinforced concrete. Mater Struct. 2011;44:1093–111.
10. Soroushian P, Lee C-D. Distribution and orientation of fibers in steel fiber reinforced concrete. ACI Mater J. 1990;87:433–9.
11. Pourzarabi A, Colombo M, Di Prisco M. On the mechanical response of a fibre reinforced concrete redundant structure; the redistribution factor. Proc. of the 12th fib international PhD symposium in civil engineering; Berlin: Czech Technical University; 2018. p. 625–32.
12. Facconi L, Plizzari G, Minelli F. Elevated slabs made of hybrid reinforced concrete: proposal of a new design approach in flexure. Struct Concr. 2019;20(1):52–67.
13. di Prisco M, Colombo M, Pourzarabi A. Biaxial bending of SFRC slabs: is conventional reinforcement necessary? Mater Struct. 2019;52:1.
14. Meda A, Minelli F, Plizzari GA. Flexural behaviour of RC beams in fibre reinforced concrete. Compos Part B Eng. 2012;43(8):2930–7.
15. Tiberti G, Minelli F, Plizzari G. Cracking behavior in reinforced concrete members with steel fibers: a comprehensive experimental study. Cem Concr Res. 2015;68:24–34.
16. Leporace-Guimil B, Mudadu A, Conforti A, Plizzari GA. Influence of fiber orientation and structural-integrity reinforcement on the flexural behavior of elevated slabs. Eng Struct. 2022;252:113583. https://doi.org/10.1016/j.engstruct.2021.113583
17. Colombo M, Martinelli P, di Prisco M. On the evaluation of the structural redistribution factor in FRC design: a yield line approach. Mater Struct. 2017;50:100.
18. di Prisco M, Martinelli P, Dozio D. The structural redistribution coefficient K_{Rd}: a numerical approach to its evaluation. Struct Concr. 2016;17:390–407.
19. di Prisco M, Colombo M, Pourzarabi A. Yield line design for SFRC elevated slabs. Proc. X RILEM-fib international symposium on fibre reinforced concrete (BEFIB), Berlin: Springer Science and Business Media B.V.; 2021.
20. Gebreyesus YY, Karinski YS, Dancygier AN, di Prisco M. Experimental investigation of cracking localization in RC beams with steel fibers. Struct Concr. 2022;24:1386–401.
21. fib. Model code for concrete structures 2020. Lausanne: International Federation for Structural Concrete; 2023 (draft of May 2023).
22. CEN. Eurocode 2: Design of concrete structures – Part 1–1: General rules – Rules for buildings, bridges and civil engineering structures. Brussels (draft of August 2022): European Committee for Standardization (CEN); 2022.

AUTHOR BIOGRAPHIES

Matteo Colombo, Associate Professor, Department of Civil and Environmental Engineering, Politecnico di Milano, Milan, Italy. Email: matteo.colombo@polimi.it

Antonio Conforti, Associate Professor, Department of Civil, Environmental, Architectural Engineering and Mathematics, University of Brescia, Brescia, Italy. Email: antonio.conforti@unibs.it

Marco di Prisco, Full Professor, Department of Civil and Environmental Engineering, Politecnico di Milano, Milan, Italy. Email: marco.diprisco@polimi.it

Bruno Leporace-Guimil, Postdoctoral Researcher, Department of Civil and Environmental Engineering, Universitat Politècnica de Catalunya, Barcelona, Spain. Email: bruno.leporace@upc.edu

Giovanni Plizzari, Full Professor, Department of Civil, Environmental, Architectural Engineering and Mathematics, University of Brescia, Brescia, Italy. Email: giovanni.plizzari@unibs.it

Giulio Zani, Assistant Professor, Department of Civil and Environmental Engineering, Politecnico di Milano, Milan, Italy. Email: giulio.zani@polimi.it

How to cite this article: Colombo M, Conforti A, di Prisco M, Leporace-Guimil B, Plizzari G, Zani G. The basis for ductility evaluation in SFRC structures in MC2020: An investigation on slabs and shallow beams. Structural Concrete. 2023; 24(4):4406–23. https://doi.org/10.1002/suco.202300114